ELSEVIER

Journal of Power Sources 66 (1997) 141–145

JOURNAL OF POWER SOURCES

Lithium state diagram as a description of lithium deposit morphology

Sergey V. Sazhin *, Mikhail Yu. Khimchenko, Yevgeniy N. Tritenichenko, Whanjin Roh, Hong Yol Kang

Samsung Display Devices Co., Energy R&D Center, 575, Shin-Dong, Paldal-Gu, Suwon City, Kyungki-Do, 442-390 South Korea

Received 14 October 1996; accepted 18 October 1996

Abstract

Lithium cycling behaviour on stainless steel has been investigated in several $LiPF_6$ and $LiClO_4$ organic electrolyte solutions. Complex dependence of cycling efficiency from a plated charge is found. In most $LiPF_6$ electrolyte solutions, cycling efficiency increases slightly with the amount of plated lithium at the lower end range of plated capacity. The critical point of the plated charge has been found for each electrolyte solution over which the cycling efficiency decreases and depends strongly on the plated charge. A 1 M $LiClO_4$/ethylene carbonate electrolyte solution displays quite different behaviour. New parameters are established for the characterization of lithium cycleability. On the basis of this research, using new parameters, a diagram of the lithium state on the amount of plated lithium is proposed for a description of the lithium deposit morphology. This diagram consists of regions of electrochemically active lithium, corrosion and encapsulation losses. Encapsulation losses can consist of (i) a loss of simple shape dendrites, and (ii) a loss of dendrite overstructure. The diagram shows a sub-region of active lithium in the region of electrochemically active lithium instead of a region of dendrite overstructure losses in the case of formation of the electron-conductive SEI.

Keywords: Lithium electrodeposition; Surface film; Morphology; Electrolytes

1. Introduction

To date, cycling efficiency has usually been used to characterize lithium anode cycleability [1–3]. Cycling efficiency allows the capacity of electrochemically active lithium to be distinguished from lost capacity that is the result of corrosion and encapsulation processes. It is impossible to discern corrosion losses from encapsulation losses using only the cycling efficiency concept. Furthermore, cycling efficiency is not constant because it depends on assigned cycling conditions such as current density and plated charge. Therefore, it is very difficult to compare results that were obtained under different conditions by various authors.

In order to obtain a clearer view, spectral studies are widely used for confirmation of the dendrite structure of lithium deposits and for finding correlations between dendrite morphology and cycling efficiency. At the same time, it is necessary to realize that scanning electron microscopy (SEM) allows the estimation of dendrite formation qualitatively rather than quantitatively. The problem of quantitative estimation of all losses during the charge/discharge process is still not solved. Considering previous research [4,5], this work attempts to describe lithium cycling behaviour quantitatively using more accurate criteria than cycling efficiency. These criteria are independent of the cycling current and plated charge and reflect only electrolyte properties. It is believed that such an approach can provide a new insight into the characteristics of the lithium electrode/electrolyte interface.

2. Experimental

Solutions of 1 M $LiPF_6$ and $LiClO_4$ solutes in different solvents (Mitsubishi Chemical) were used mainly as received. Some of the solutions were prepared in the authors' laboratory from $LiPF_6$ and $LiClO_4$ (Kishida Chemical) dissolved in organic solvents (Mitsubishi Chemical). Water content was measured by a Mettler Toledo DL37 KF coulometer and was in the range 14 to 35 ppm in these solutions. Lithium metal (99.9%, Aldrich) in the form of a thin sheet was employed as a counter electrode. Solution preparation, cell assembly, etc., were carried out in a highly pure argon atmosphere in a Vacuum Atmospheres Company (VAC) glove box.

* Corresponding author. Fax: +82 (331) 210-7760; e-mail: sazhin@sdd.samsung.co.kr.

PII S0378-7753(96)02542-6

The experiments were carried out using two-electrode cells. A sealed 2016 coin cell was used as a cell testing vehicle. The coin cell casing material was stainless steel. The surface area of the working electrode (the empty can of the coin cell) was 2 cm^2. The counter electrode was a lithium sheet (2 cm^2) that was plated into the cover of the coin cell. A microporous membrane (3M Company) was used as a separator.

The electrochemical cells were cycled galvanostatically at different currents at 50 °C using a battery charge/discharge testing unit 'TOSCAT-3000U/3100U' (Toyo System). The charge and discharge currents were the same. The cut-off voltage for lithium stripping was 0.6 V. The plating time was the same at the different currents and was equal to 5 min. Each cell performed at one current only for four cycles. The average coulombic cycling efficiency from the second to the fourth cycle was calculated for each current. In order to overcome irreproducibility, three identical experiments at each current were carried out. The best average cycling efficiency from the three attempts was used for further processing and plotting.

The dependencies of capacity loss rate (j_l) on the plated charge (Q_p) were plotted for new cycling parameters' determination. The rate of capacity loss was calculated from

$$j_l = (Q_p - Q_s)/(t_p + t_s) = Q_p(100 - E)/t_p(100 + E) \quad (1)$$

where Q_p and t_p are the capacity (C cm^{-2}) and time (s) of plating; Q_s and t_s are the capacity and time of stripping; $E = Q_s/Q_p$ is the coulombic efficiency (%).

The method of least squares was used for j_l–$j_l(Q_p)$ dependencies plotting at the restriction $(j_l)_j^{calc} \leq (j_l)_j^{exp}$. The reason for using such a restriction was to find the level at which as much compact lithium deposit as possible, over several attempts, could be plated in certain electrolyte solutions.

3. Results and discussion

Investigations show that the cycling behaviour of lithium in different solutions with $LiPF_6$ solute is similar. By way of example, the experimental results in the j_l–$j_l(Q_p)$ and E–$E(Q_p)$ axis for the 1 M $LiPF_6$/EC + DEC (1:2.6) electrolyte solution are presented in Fig. 1. The dependence of E–$E(Q_p)$ has a complex form that consists of two parts, I and II.

The corresponding graph of j_l–$j_l(Q_p)$ is more simple and consists of two lines. For the sake of simplicity, discussion is started from the j_l–$j_l(Q_p)$ graph explanation. Line I of the j_l–$j_l(Q_p)$ graph at the lower end range of the charges is described by the equation

$$j_l = j_c + \gamma Q_p/t_p \quad (2)$$

where j_c is a segment on the capacity loss rate axis that is intersected by line I and γ/t_p is the incline of line I. At this end range of the plated charge, the lithium deposit is relatively smooth and the dendrites have a simple form. Beginning with a certain critical plated charge (Q_p^{crit}), the slope of j_l–$j_l(Q_p)$ dependence rises considerably. This can be explained as follows. It is believed that at $Q_p > Q_p^{crit}$, the dendrite overstructure can be formed during charge. This promotes additional losses during the entire charge/discharge procedure. The overstructure can be represented as branch-form dendrites that grow on the surface of primary dendrites. During discharge, in the case of contact damage at the bottom of such complex branch-form dendrites, the encapsulated capacity loss will be higher than in the case of simple-shape dendrites.

Line II of the graph j_l–$j_l(Q_p)$ at $Q_p > Q_p^{crit}$ can be described as analogous to Eq. (2)

$$j_l = j_c + \gamma Q_p/t_p + \beta(Q_p - Q_p^{crit})/t_p$$
$$= j_c - \beta Q_p^{crit}/t_p + (\gamma + \beta)Q_p/t_p \quad (3)$$

where $(\gamma + \beta)/t_p$ is an incline of line II.

Using the Eqs. (1) and (2), part I of the $E = E(Q_p)$ dependence (Fig. 1) can be represented by

$$E = \{[Q_p(1 - \gamma) - j_c t_p]/[Q_p(1 + \gamma) + j_c t_p]\} \times 100\% \quad (4)$$

In the same manner, using the Eqs. (1) and (3), part II of the $E = E(Q_p)$ dependence can be described by

$$E = \{[Q_p(1 - \gamma - \beta) + \beta Q_p^{crit} - j_c t_p]/$$
$$[Q_p(1 + \gamma + \beta) - \beta Q_p^{crit} + j_c t_p]\} \times 100\% \quad (5)$$

The coefficients j_c, γ, β, Q_p^{crit} in Eqs. (1)–(5) are the new parameters of lithium cycleability or the electrolyte testing parameters. Their physical meaning can be explained as follows:

1. j_c ($j_c \geq 0$): corrosion current density (the rate of decomposition of electrolyte solution components, that is, the measure of the passivating properties of the surface film);
2. γ ($0 \leq \gamma \leq 1$): encapsulation degree of simple-shape dendrites (the degree of the 'dead' dendriteability of the electrolyte solution, which means the ability of the electrolyte solution to create 'dead' dendrites of simple shape during the charge/discharge conditions). 'Dead' dendrites are dendrites that have lost electrical contact with the electrode bulk;

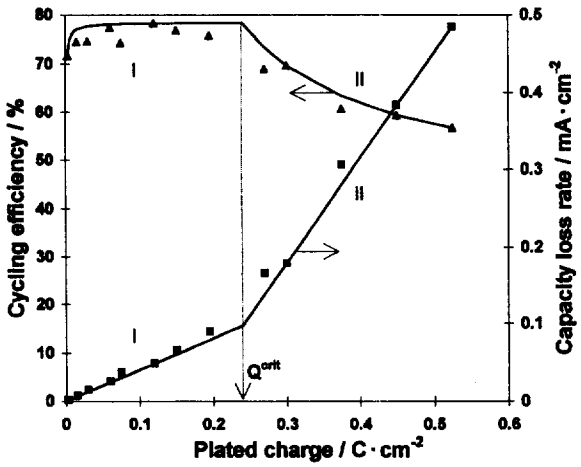

Fig. 1. Dependence of cycling efficiency and capacity loss rate of electrodeposited lithium on amount of plated lithium in 1 M $LiPF_6$/EC + DEC (1:2:6) electrolyte solution.

Table 1
Parameters of 1 M electrolyte solutions for lithium cycling on stainless-steel substrate at 50 °C

Electrolyte solution			Electrochemical parameters			
Salt	Solvent	Water content (ppm)	$j_c \times 10^4$ (mA cm^{-2})	γ	β	Q_p^{crit} (C cm^{-2})
$LiPF_6$	EC–DMC (1:1)	16	4.1	0.110	0.256	0.192
	EC–DEC (1:1)	20	20	0.121	0.017	0.150
	EC	23	2.3	0.053	0.145	0.099
	EC–DEC (1:2.6)	14	4.4	0.121	0.286	0.240
	DMC	15	1.1	0.107	0.095	0.071
	DEC	30	Strong interaction with lithium. Reduction products are solid and liquid of reddish-brown colour. It is impossible to find electrochemical parameters because of the very high resistance of the passive film.			
$LiClO_4$	EC	24	152	0.340	−0.287	0.340
	PC	21	8.9	0.483	0.337	0.221
	EC–DEC (1:1)	35	3.9	0.333	0.299	0.090
$LiClO_4$–$LiPF_6$ (1:1)	EC	26	21.9	0.161	0.132	0.184

3. β: encapsulation degree of dendrite overstructure which means the ability of the electrolyte solution to create dendrite overstructure (at $\beta > 0$: 'dead' dendrite overstructure and at $\beta < 0$: electrochemically active dendrite overstructure), and
4. Q_p^{crit}: critical plated charge (the charge value when characters of the deposit structure are changed qualitatively).

It is clear from the results presented in Fig. 1 that the lithium cycling efficiency increases slightly with the plated charge at its lower end. It deals with the fact that the corrosion current is sufficiently small and the encapsulation process (γ) does not depend on the plated charge, only on the nature of the electrolyte solution. The cycling efficiency decreases strongly with the plated charge at $Q_p > Q_p^{crit}$.

Electrochemical parameters for eight electrolyte solutions are summarized in Table 1. Although the behaviour of all $LiPF_6$ electrolyte solutions is similar, the values of testing parameters are different. At the same time, it is necessary to emphasize that the behaviour of the 1 M $LiClO_4$/EC electrolyte solution is completely different from that of the others (see Fig. 2). Overvoltage during charge/discharge procedure in this electrolyte is lower than in other electrolytes. The corrosion current is 7 to 60 times higher than in others, while the content of water is almost the same. The critical charge is also higher, but the main discrepancy is the absence of additional encapsulation after critical charge. Moreover, the cycling efficiency (Fig. 2) improves remarkably at $Q_p > Q_p^{crit}$ and the slope of line II of the j_l–$j_l(Q_p)$ graph is lower than that of line I ($\beta < 0$).

A complex of such unusual properties of this electrolyte can be explained as follows. As expected [6–10], interfacial properties are highly dependent on the combination of salt(s)–solvent(s)–additive(s) used, because the chemical composition of the produced film is heterogeneous, containing different types of Li-ion and electron conductors. Therefore, the electronic properties of the surface films which they induced upon cycling and character of lithium morphology depends on their occasional chemical composition [11]. In connection with this we hypothesize that the produced composite film in the 1 M $LiClO_4$/EC electrolyte solution possesses sufficient electronic conductivity. The electronic conductivity of the film decreases the interfacial resistance (overvoltage becomes lower), promotes the corrosion via electron transfer through the film (large corrosion current), and causes an increase in the yield of capacity during discharge (cycling efficiency increasing) after critical capacity destination. Increase in cycling efficiency is due to the surface electric contact between the branches of the dendrite overstructure.

From the practical point of view, those electrolytes that produce highly protective solid electrolyte interfaces (SEI) are preferable. This means that the corrosion current should be low. According to other parameters, the larger is the Q_p^{crit} and the lower are the γ and β modulus, the better is the electrolyte.

According to Eq. (2), the capacity loss rate at $Q_p < Q_p^{crit}$ consists of two terms: the corrosion rate j_c and the 'dead'

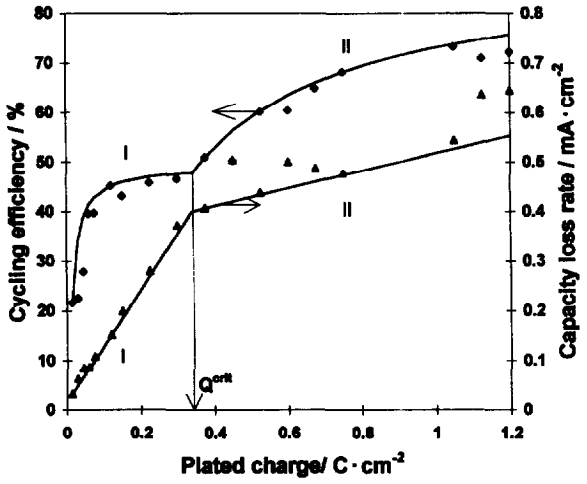

Fig. 2. Dependence of cycling efficiency and capacity loss rate of electrodeposited lithium on amount of plated lithium in 1 M $LiClO_4$/EC electrolyte solution.

dendrite formation rate $\gamma Q_p/t_p$ for simple-shape dendrites. The additional 'dead' dendrite formation rate $\beta(Q_p-Q_p^{crit})/t_p$ for dendrite overstructure is added too at $Q_p > Q_p^{crit}$ (see Eq. (3)). When the partial rates are known, it is possible to calculate the partial percentage capacity loss values. At $Q_p < Q_p^{crit}$, the percentage corrosion losses are $\{j_c(t_p+t_s)/Q_p\}100\% = \{j_c t_p(E+1)/Q_p\}100\% = \{2j_c t_p/[Q_p(1+\gamma)+j_c t_p]\}100\%$ and the encapsulation losses for simple-shape dendrites are $\{\gamma Q_p(t_p+t_s)/t_p Q_p\}100\% = \{\gamma(E+1)\}\times 100\% = \{2\gamma Q_p/[Q_p(1+\gamma)+j_c t_p]\}100\%$. At $Q_p > Q_p^{crit}$, the percentage corrosion losses are $\{j_c(t_p+t_s)/Q_p\}100\% = \{j_c t_p(E+1)/Q_p\}100\% = \{2j_c t_p/[Q_p(1+\gamma+\beta)-\beta Q_p^{crit}+j_c t_p]\}100\%$, the losses for simple-shape dendrites are $\{\gamma Q_p(t_p+t_s)/t_p Q_p\}100\% = \{\gamma(E+1)\}100\% = \{2\gamma Q_p/[Q_p(1+\gamma+\beta)-\beta Q_p^{crit}+j_c t_p]\}100\%$ and the dendrite overstructure losses are $\{\beta(Q_p-Q_p^{crit})(t_p+t_s)/t_p Q_p\}\times 100\% = \{\beta(Q_p-Q_p^{crit})(E+1)/Q_p\}100\% = \{2\beta(Q_p-Q_p^{crit})/[Q_p(1+\gamma+\beta)-\beta Q_p^{crit}+j_c t_p]\}100\%$.

Using the percentage capacity loss values, as well as the values of the cycling efficiency at the different plated charges, the lithium state diagram can be plotted. Fig. 3 presents this kind of diagram as a result of the computer simulations at $\beta > 0$ and with a sufficiently high level of corrosion current. An artificial case is used in order to show clearly all diagram regions, especially the corrosion region. In this diagram, three main regions can be seen. The region of the corrosion losses is separated from the region of the encapsulation losses by the curves II and V. The curve II is described by $Y_{II} = \{[Q_p(1+\gamma)-j_c t_p]/[Q_p(1+\gamma)+j_c t_p]\}100\%$, and the curve V by the equation $Y_V = \{[Q_p(1+\gamma+\beta)-\beta Q_p^{crit}-j_c t_p]/[Q_p(1+\gamma+\beta)-\beta Q_p^{crit}+j_c t_p]\}100\%$. The region of the encapsulation losses is divided into two parts by curve IV, which is described by $Y_{IV} = \{[Q_p(1-\gamma+\beta)-\beta Q_p^{crit}-j_c t_p]/[Q_p(1+\gamma+\beta)-\beta Q_p^{crit}+j_c t_p]\}100\%$. One part is a sub-region of losses of simple-shape dendrites and another is a sub-region of losses of the dendrite overstructure. The last region is electrochemically active lithium. This region is separated from the region of encapsulation losses by the curves I and III that are described by the Eqs. (4) and (5), respectively. The diagram clearly displays that corrosion takes away not only at the active lithium, but also at the encapsulated lithium. Dendrite overstructure losses engulf the part of the losses of simple-shape dendrites.

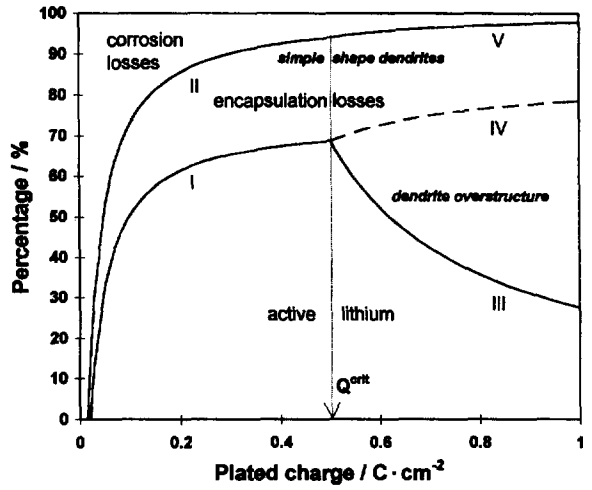

Fig. 3. Diagram of the lithium state during cycling on the amount of plated lithium at $\beta > 0$. $j_c = 0.03$ mA cm^{-2}, $\gamma = 0.15$, $Q_p^{crit} = 0.5$ C cm^{-2}, $\beta = 0.8$, and $t_p = 10$ min.

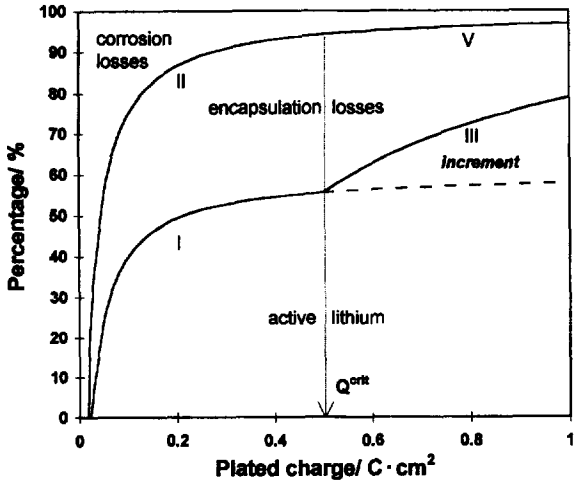

Fig. 4. Diagram of lithium state during cycling on the amount of plated lithium at $\beta > 0$. $j_c = 0.03$ mA cm^{-2}, $\gamma = 0.25$, $Q_p^{crit} = 0.5$ C cm^{-2}, $\beta = -0.3$, and $t_p = 10$ min.

At $\beta < 0$, the diagram of the lithium state has a quite different construction, as presented in Fig. 4. It does not contain the sub-region of the losses of the dendrite overstructure. Instead, it contains the sub-region of active lithium in the region of electrochemically active lithium. Since dendrite overstructure is electrochemically active in this case, line IV loses its physical meaning and is absent from the diagram.

All regions on the diagrams are interdependent. Changing of one parameter provokes changing all of regions.

4. Conclusions

Lithium cycling behaviour on stainless steel in different electrolyte solutions is complex and sometimes quite different. Lithium behaviour is similar in solutions with $LiPF_6$ solute. In most of them, cycling efficiency increases slightly with the amount of plated lithium at the lower end range of the plated charge. A critical point of the plated charge is found at which the lithium deposit behaviour is changed radically. After this point, the cycling efficiency decreases and depends strongly on the plated capacity. At the same time, quite different lithium deposit behaviour is found in the 1 M $LiClO_4$/EC electrolyte solution. It is hypothesized that the electronic conductivity of the produced surface film is responsible for this change in behaviour.

In order to find a mathematical description for lithium cycling peculiarities, it is proposed to present experimental results in the j_l–$j_l(Q_p)$ axis and to use the combination of two equations: $j_l = j_c + \gamma Q_p/t_p$ and $j_l = j_c - \beta Q_p^{crit}/t_p + (\gamma+\beta)Q_p/t_p$. The coefficients j_c, γ, β, Q_p^{crit} in these equations are

suitable criteria to characterize the electrolyte and the lithium deposit morphology. Values of these electrolytes testing parameters in eight electrolyte solutions with $LiClO_4$ and $LiPF_6$ solutes have been determined.

Using the proposed criteria, the diagram of the lithium state on the amount of plated lithium is presented. This diagram describes the regions of the active lithium, corrosion and encapsulation losses. Encapsulation losses can consist of: (i) a loss of simple-shape dendrites, and (ii) a loss of dendrite overstructure. In the case of formation of the electron-conductive SEI, the diagram may contain a sub-region of active lithium in the region of electrochemically active lithium instead of a region of dendrite overstructure losses.

The lithium state diagram is eminently suitable to describe quantitatively the lithium deposit morphology.

5. List of symbols

E	cycling efficiency, %
j_l	capacity loss rate, A cm^{-2}
$(j_l)_j^{exp}$	experimental value of capacity loss rate at j current density, A cm^{-2}
$(j_l)_j^{calc}$	calculated value of capacity loss rate at j current density, A cm^{-2}
j_c	corrosion current density, A cm^{-2}
Q_p	plated charge, plated capacity, C cm^{-2}
Q_p^{crit}	critical plated charge, critical plated capacity, C cm^{-2}
Q_s	stripped charge, stripped capacity, C cm^{-2}
t_p	plating time, s
t_s	stripping time, s

Greek letters

γ	encapsulation degree of simple-shape dendrites
β	encapsulation degree of dendrite overstructure

Abbreviations

SEI	solid electrolyte interface
EC	ethylene carbonate
PC	propylene carbonate
DMC	dimethyl carbonate
DEC	diethyl carbonate

References

[1] R.D. Rauh and S.B. Brummer, *Electrochim. Acta*, 22 (1977) 75.
[2] S.-I. Tobishima and A. Yamaji, *Electrochim. Acta*, 28 (1983) 1067.
[3] J.L. Goldman, R.M. Mank, J.H. Young and V.R. Koch, *J. Electrochem. Soc.*, 127 (1980) 1461.
[4] S.V. Sazhin, A.V. Gorodyskii, M.Y. Khimchenko, S.P. Kuksenko and V.V. Danilin, *J. Electroanal. Chem.*, 344 (1993) 61.
[5] S.V. Sazhin, A.V. Gorodyskii and M.Y. Khimchenko, *J. Power Sources*, 47 (1994) 57.
[6] D. Aurbach, A. Zaban, A. Schechter, Y. Ein-Eli, E. Zinigrad and B. Markovsky, *J. Electrochem. Soc.*, 142 (1995) 2873.
[7] D. Aurbach and O. Chusid, *J. Electrochem. Soc.*, 140 (1993) L1.
[8] K. Kanamura, S. Shiraishi, H. Tamura and Z. Takehara, *J. Electrochem. Soc.*, 141 (1994) 2379.
[9] C. Nanjundia, J.L. Goldman, L.A. Dominay and V.R. Koch, *J. Electrochem. Soc.*, 135 (1994) 2914.
[10] M. Froment, M. Garreau, J. Thevenin and D. Warin, *J. Microsc. Spectrosc. Electron.*, 4 (1979) 111; 483.
[11] Y. Ein-Eli and D. Aurbach, *J. Power Sources*, 54 (1995) 281.